J Biomol NMR (2017) 68:53–63
DOI 10.1007/s10858-017-0114-9

ARTICLE

Impact of spin label rigidity on extent and accuracy of distance information from PRE data

K. A. Schnorr[1] · D. B. Gophane[2] · C. Helmling[1] · E. Cetiner[1] · K. Pasemann[1] · B. Fürtig[1] · A. Wacker[1] · N. S. Qureshi[1] · M. Gränz[3] · D. Barthelmes[1] · H. R. A. Jonker[1] · E. Stirnal[1] · S. Th. Sigurdsson[2] · H. Schwalbe[1]

Received: 8 March 2017 / Accepted: 3 May 2017 / Published online: 12 May 2017

Abstract Paramagnetic relaxation enhancement (PRE) is a versatile tool for NMR spectroscopic structural and kinetic studies in biological macromolecules. Here, we compare the quality of PRE data derived from two spin labels with markedly different dynamic properties for large RNAs using the I-A riboswitch aptamer domain (78 nt) from *Mesoplamsa florum* as model system. We designed two I-A aptamer constructs that were spin-labeled by noncovalent hybridization of short spin-labeled oligomer fragments. As an example of a flexible spin label, ^{Ureido}U-TEMPO was incorporated into the 3′ terminal end of helix P1 while, the recently developed rigid spin-label Çm was incorporated in the 5′ terminal end of helix P1. We determined PRE rates obtained from aromatic ^{13}C bound proton intensities and compared these rates to PREs derived from imino proton intensities in this sizeable RNA (~78 nt). PRE restraints derived from both imino and aromatic protons yielded similar data quality, and hence can both be reliably used for PRE determination. For NMR, the data quality derived from the rigid spin label Çm is slightly better than the data quality for the flexible ^{Ureido}TEMPO as judged by comparison of the structural agreement with the I-A aptamer crystal structure (3SKI).

Keywords Paramagnetic NMR · EPR · RNA · Spin labeling · Paramagnetic relaxation enhancement (PRE)

Introduction

In NMR and EPR studies, paramagnetic spin labels serve as versatile probes for structural biology studies (Otting 2010a; Krstic et al. 2012). As a result of the ~700 times larger magnetic moment of an electron compared to protons, long-range distance restraints extracted from quantification of paramagnetic relaxation enhancement can supplement conventional NOE based data (<6 Å) (Schmidt and Kuntz 1984; Bertini and Luchinat 1999; Bertini et al. 2008, 2012; Madl et al. 2011). Due to their sensitivity, paramagnetic relaxation enhancements (PREs) can provide insight into nonspecific encounter complexes (Iwahara et al. 2004; Blundell and Fernández-Recio 2006; Tang et al. 2006), allow characterization of transient lowly populated states (Tang et al. 2008; Clore and Iwahara 2009), and enable mapping of the conformational space (Ubbink et al. 2002; Tang et al. 2007; Otting 2010b; Guan et al. 2013). However, the incorporation of the paramagnetic species into the biomolecule remains a major challenge for PRE NMR while keeping both structure and function intact. The introduction of nitroxide-based tags into proteins via cysteine residues (Kosen 1989; Gillespie and Shortle 1997; Battiste and Wagner 2000; Gaponenko et al. 2000), encodable lanthanide binding tags (LBTs) (Wöhnert et al. 2003; Barthelmes et al. 2011), or chemically attached metal-ion

Electronic supplementary material The online version of this article (doi:10.1007/s10858-017-0114-9) contains supplementary material, which is available to authorized users.

✉ H. Schwalbe
schwalbe@nmr.uni-frankfurt.de

[1] Center for Biomolecular Magnetic Resonance (BMRZ), Institute of Organic Chemistry and Chemical Biology, Johann Wolfgang Goethe-Universität, Max-von-Laue Strasse 7, 60438 Frankfurt am Main, Germany

[2] Department of Chemistry, Science Institute, University of Iceland, Dunhaga 3, 107 Reykjavik, Iceland

[3] Center for Biomolecular Magnetic Resonance (BMRZ), Institute of Physical and Theoretical Chemistry, Johann Wolfgang Goethe-Universität, Max-von-Laue Strasse 7, 60438 Frankfurt am Main, Germany

chelators (Donaldson et al. 2001; Dvoretsky et al. 2002; Pintacuda et al. 2004; Graham et al. 2011), is well established and widely applied (Liang et al. 2006; Hubbell et al. 2013). Site-directed spin labeling methods and their application for RNA, however, are comparatively rare. Although NMR structural and dynamic investigation of large RNAs are increasingly pursued, only few PRE studies on site-specifically labeled RNA have been reported to date (Ramos and Varani 1998; Wunderlich et al. 2013; Helmling et al. 2014; Lebars et al. 2014).

Functional non-coding RNAs are involved in diverse cellular processes, such as RNA–protein interactions in ribosomes (Carter et al. 2000) and spliceosome (Li et al. 2009; Mourão et al. 2016; Bertram et al. 2017), catalytic activities in ribozymes (Sashital and Butcher 2007), or genetic control in riboswitches (Breaker 2011; Serganov and Nudler 2013). Understanding the underlying mechanistic principles makes structural and dynamic investigations of these RNAs and their subcomplexes very interesting, yet challenging. In this context, PRE NMR can provide information on long-ranging conformational changes up to 35 Å to complement short-range restraints obtained from NOEs yielding structural restrains within the 5–6 Å range (Iwahara et al. 2007b). In long and elongated helical segments of RNA molecules, where NOE interactions are limited, PRE NMR can furthermore provide helpful long-range information and reveal interhelical tertiary structural motions where the short ranging NOE is often limited.

Compared to spin labeling of proteins, such application for nucleic acids remains challenging due to the requirement of chemical synthesis to incorporate modifications. Therefore, the preparation of spin-labeled RNA is very costly and also sometimes infeasible for oligomers/RNAs >40 nt. Nitroxide labeling of chemically synthesized nucleic acids has been mainly developed for EPR studies, where comparably small amounts of material are needed (~2 nmol for cw-EPR vs. ~150 nmol for NMR). Several approaches for spin labeling at different sites have been reported in the literature. Site-specific introduction of nitroxides has been accomplished by solid-phase synthesis, introducing chemically modified phosphoramidites containing the paramagnetic group (Spaltenstein et al. 1988). Alternatively, convertible nucleosides have been used (Allerson et al. 1997; Sicoli et al. 2010; Höbartner et al. 2012) to incorporate the paramagnetic group post-synthetically (Macosko et al. 1999; Lebars et al. 2014). Possible sites for spin labeling have been reported at the RNA backbone (Nagahara et al. 1992), the nucleobase (Qin et al. 2003; Piton et al. 2007; Shelke and Sigurdsson 2012), at the sugar ring (Edwards et al. 2001; Saha et al. 2015), and at the 5′- (Macosko et al. 1999; Wunderlich et al. 2013) or 3′-terminus of RNAs (Caron and Dugas 1976). In particular, successful incorporation of spin labels has been shown on purine and pyrimidine residues with modification at position five of the base by Pd-catalyzed cross-coupling (Piton et al. 2007) or at the 2′ position of the ribose unit (Saha et al. 2015). Furthermore, noncovalent labeling strategies have been reported at abasic sites of nucleic acids (Shelke and Sigurdsson 2010; Shelke et al. 2014; Kamble et al. 2016). Recent studies using DNA- and T4 RNA-ligase-catalyzed ligation of transcribed and spin-labeled RNA fragments (Büttner et al. 2013; Lebars et al. 2014) show alternative ways to spin label RNAs, perfectly suited for EPR quantities. These methods, however, are comparably costly for the production of amounts needed in NMR studies, and further require advanced chemistry and individual optimization for every construct under investigation.

Here, we apply a previously established noncovalent spin labeling strategy (Helmling et al. 2014) for the I-A aptamer (78 nt) from *Mesoplasma florum* (Kim et al. 2007), and incorporate two spin labels with different dynamic properties to compare structural restraints obtained from PRE NMR. We further compare PRE data derived from ^{15}N- vs. ^{13}C-bound protons to investigate whether solvent exchange of imino protons can introduce a systematic error on the transversal PRE rate Γ_2. The spin label was incorporated into the RNA by hybridizing a short spin-labeled oligomer fragment (10 nt) to a larger RNA (68 nt). Our data show that valuable information can be obtained from spin-labeled RNA and that rigidity of spin labels has a modest effect on structural data derived for NMR applications.

Materials and methods

RNA transcription, purification and sample preparation

Truncated RNA aptamers (68 nt) were prepared enzymatically from linearized plasmids by in vitro transcription (Stoldt et al. 1998), and were further purified via HPLC. For transcription of the I-A aptamer with the truncated 5′-end (68 nt), we used a 5′-hammerhead ribozyme (99 nt), and for transcription of the 3′-truncated I-A aptamer, a 3′-hepatitis delta virus (HDV) ribozyme was used. RNAs were homogeneously folded by 5 min. denaturation at 95 °C and concentrations of ~0.2 mM, followed by dilution with ten equiv. of ice-cold water and refolding on ice for 1 h. The RNA was then exchanged into NMR buffer (25 mM potassium phosphate, 50 mM potassium chloride, pH 6.2) in centrifugal concentrators (Vivaspin, MWCO: 5000, Sartorius; 10 min., 6500×*g*, 4 °C). The purified and folded RNA was maintained at 4 °C to allow hybridization with the spin-labeled oligomer fragments. The oligomer fragment containing the rigid ring-fused nucleobase label, Çm, was synthesized by solid-phase synthesis (Shelke and

Sigurdsson 2012; Höbartner et al. 2012). The oligomer fragment (10 nt) containing the flexible ^{Ureido}U-TEMPO group was prepared from 2′-amino (U) modified oligomer (Thermo Scientific Dharmacon) and 4-Isocyanato-TEMPO from precursor 4-amino-TEMPO (Sigma-Aldrich), according to (Edwards and Sigurdsson 2007).

Gel shift assays

We performed polyacrylamide gel electrophoresis (PAGE) under native conditions to identify homogeneous folding of the purified RNA constructs and to investigate hybridization of the spin-labeled oligomer fragments. 12% polyacrylamide gels were run at 298 and 277 K with a running buffer composed of tris acetate (pH 8.0, 50 mM) and sodium acetate (100 mM). The applied power was kept below 1.5 W and water cooling was applied to prevent overheating. Gels were stained by incubation in GelRed™ (Biotium) for 15 min. and digitalized on a Gel iX imager (Intas).

Continuous wave (CW) EPR experiments

We performed CW-EPR measurements to analyze the spin labeling efficiency and the degree of hybridization of the oligomer fragments to the truncated I-A aptamer. Acquisition of spectra, simulation and fitting were performed using *EasySpin* (*Matlab Toolbox*) (Stoll and Schweiger 2006). Spectra were acquired in a sample volume of 20 µL containing 100 µM of 68mer, 1.2 equiv. of 10mer, 2 equiv. of 2′-deoxyguanosine (2′-dG), and 8 equiv. of Mg^{2+}. CW-EPR measurements were performed at X-band frequencies (9.54 GHz) using a Bruker E500 spectrometer equipped with a TE102 cavity. Experimental parameters were set to 100 kHz modulation frequency, 0.1 mT modulation amplitude, 0.2 mW microwave power, 40.96 ms time constant, 40.96 ms conversion time, 1024 points, 7 mT sweep width, 20 scans. The EPR signal was acquired as the first derivative of the absorption signal. Fitting with EasySpin was performed assuming an isotropic model for the isolated TEMPO group and an anisotropic model for the isolated Çm group and spin label coupled to the oligomer fragments alone and hybridized to the 68mer fragments.

Prediction of palindromicity and hybridization energies

We predicted palindromicity and hybridization energies for up to 1024 oligomers, generated in Mathematica (Wolfram research) and determined their Gibbs energies for hybridization to the complement P1 sequence using the software *ViennaRNA* package (Mückstein et al. 2006) (Supplementary Table S1). Furthermore, we determined the Gibbs energies for 10mer-10mer duplex formation to screen decamers with the lowest possible tendency to form dimer due to (partial) palindromicity (Supplementary Table S2).

NMR experiments

The RNA samples were prepared in NMR buffer (25 mM K_2HPO_4/KH_2PO_4, 50 mM KCl, pH 6.2) containing 10% of D_2O. For each construct, 1.2 equiv. of oligomer, 2 equiv. of 2′-dG and 8 equiv. of Mg^{2+} were added. The final sample volume of 280 µL further contained ~180 µM DSS as reference. PRE experiments measured on 350 µM samples with 1.2 equiv. of spin-labeled oligomer to avoid intermolecular PREs. We used the slight excess of the spin label to compensate for errors in the concentration determination. Spin labels were reduced by adding 2 equiv. of freshly prepared ascorbic acid. All NMR experiments were measured on Bruker AV600, AV700, and AV800 NMR spectrometer equipped with a 5 mm z-axis gradient TXI-HCN cryogenic probe. Processing of data was performed using the software Topspin 2.1, 3.2, 3.5 (Bruker BioSpin) and analysed with Sparky 3.114 (Goddard and Kneller 2008).

PRE rates and distance calculation

We measured two time-point experiments to determine transversal PRE rates on ^{13}C- and ^{15}N-bound protons derived from signal intensities, as reported in the literature (Iwahara et al. 2007b). The presented two-time point approach has previously been discussed and does not require fitting procedures nor sophisticated error estimations. ^1H_N-Γ_2 rates derived from imino protons were acquired from interleaved ^{1}H,^{15}N-BEST-TROSY experiments with spin-echo delays of 0.008 and 8.008 ms. ^1H_C-Γ_2 rates derived from adenine-H2 intensities were acquired in a similar manner from an interleaved ^{1}H,^{13}C-HSQC type experiment, based on a standard Bruker pulse sequence (hsqcetgpsisp2). The PRE delay in the C2-H2 experiment was identical to that of the ^{1}H–^{15}N experiment: 0.008 and 8.008 ms. Experimentally determined PRE rates were converted into distances as described in the literature (Battiste and Wagner 2000; Volkov et al. 2006). The correlation time τ_c of the PRE interaction vector was extrapolated to 15.2 ns, based on the rotational correlation time for the shorter wild-type I-A aptamer of 12.9 ns, determined with HYDRONMR (Garca de la Torre et al. 2000) using the crystal structure of the I-A aptamer as structural model. For further estimation of the rotational correlation time of the PRE interaction vector, ^{1}H-R_1 and ^{1}H-R_2 measurements in the paramagnetic/diamagnetic state could be performed, as previously described (Gillespie and Shortle 1997).

Evaluation of possible spin label positions

Possible spin labelling sites were evaluated theoretically by manual addition of the ^{Ureido}TEMPO group to the RNA crystal structure with PyMOL 1.7.6.3 (DeLano and Grosse-Kunstleve). This structure was evaluated with a python 2.7 script as follows. All possible rotamers were determined by rotation of the spin label around the flexible bonds connecting the spin label and the RNA. Discarding all rotamers in which at least one distance between any atom of the RNA and any atom of the spin label was shorter than 1.5 Å, led to a rotamer ensemble that mapped the available volume of the spin label. The average position of the ensemble was subsequently used to measure the distance between the HSQC detectable nuclei and the electron. These distances were classified into three categories: <14 Å, between 14 and 23 Å and >23 Å.

Results

Construct design, palindromicity and hybridization of the oligomer fragment

The wild-type sequence of the I-A aptamer containing an extended P1 helix by seven base pairs to allows hybridization of the spin-labeled oligomer. To ensure hybridization of the oligomer, we performed computer simulations with the program RNAduplex (Lorenz et al. 2011) and screened 10mer fragments for lowest hybridization free energies and relatively high intramolecular interaction energies (Supplementary Table S1). We screened 1024 10mer sequences for the 5′-truncated 68mer and 256 oligomers for the 3′-truncated 68mer, respectively. The spin label was positioned in close proximity to the binding pocked without disturbing the hybridization of the oligomer fragment. The oligomer sequence chosen for TEMPO labeling exhibits a calculated hybridization energy of −17.6 kcal/mol and palindromicity energy of +1.3 kcal/mol. Calculated hybridization energies for the rigid Çm-labeled oligomer account for −17.4 kcal/mol and a relatively high energy of palindromicity of +3.8 kcal/mol (Supplementary Table S2).

The gel shift assay in Fig. 1c shows a clear decrease of the migration speed for the ^{Çm}10mer fragment in the presence of the 68mer fragment, suggesting formation of a stable complex. The ^{TEMPO}10mer forms a slightly less stable complex, as expected due to the larger duplex destabilization of the TEMPO label (Edwards et al. 2001) in contrast to the rigid Çm label (Höbartner et al. 2012).

To analyze the fraction of spin-labeled oligomer not bound to an RNA (called: “solo”; supplementary material), an isotropic fitting procedure was performed based on complete freedom of molecular tumbling in the unbound form, while for the analysis of rotational correlation time τ_r of the spin label bound to the 10mer fragment or the 78mer RNA, anisotropic fitting was performed. As expected, calculated τ_r values increased with the size of the molecule and rigidity of the spin label in the following order: TEMPO (solo) > Çm (solo) > ^{TEMPO}10mer > ^{Çm}10mer > ^{TEMPO}78mer > ^{Çm}78mer (Supplementary Table S3). Spin counting verified high spin labeling efficiency, and yielded concentrations in excellent agreement with those determined by UV spectroscopy (NanoDrop).

NMR characterization and structural integrity hybrids vs. wt-aptamer

Characterization of the complexes was performed by NMR spectroscopy. All solvent exchange protected imino protons of both complexes were identified by sequential walk in NOESY spectra (Fig. 2). Imino protons of U36 and U64 were broadened beyond detection. The detection of all 14 imino proton signals in helix P1 provided evidence for complete oligomer hybridization in agreement with results from native PAGE. Expected tertiary interactions in the ligand-bound states reported for U33, G38, G39 (loop–loop kissing) and G24, G46, G52 (binding pocket) were in agreement with the native I-A aptamer domain. Resonances for U27 and U41 could not be assigned unambiguously in the NOESY spectrum, but were assigned indirectly in ^{13}C-edited NOESY experiments (Supplementary Figure S5, S7). ^{15}N-TROSY and ^{13}C-HSQC experiments validated the assignment of all imino protons and aromatic adenine H2 resonances. Close structural similarity of the hybrids with the wild-type I-A aptamer (70 nt) was interfered from comparison of the resonance pattern in ^{15}N-TROSY and ^{13}C-HSQC spectra. The spin-labeled 68 + 10mer complexes showed the same conformation as the native aptamer. Characteristic reporter signals for the formation of the binding pocket (G24, G46, G52) and the resonance of the cognate ligand (2′-dG) showed full agreement in the spectral overlays. However, small chemical shift perturbations (CSP) were detected in the P1 stem caused by elongation of the lower part of the helix (Fig. 2).

PRE data

Transverse PRE rates (^{1}H-Γ_2) were determined for imino protons and aromatic adenine H2 cross peaks on the spin-labeled 68 + ^{TEMPO}10mer and 68 + ^{Çm}10mer systems. Since imino protons are well dispersed from aromatic and sugar protons, they serve as important reporter signals for RNA secondary and tertiary interactions. However, to assess the inherent problem of solvent exchange, PRE rates were also determined for aromatic non-exchangeable adenine H2 resonances. Experimental

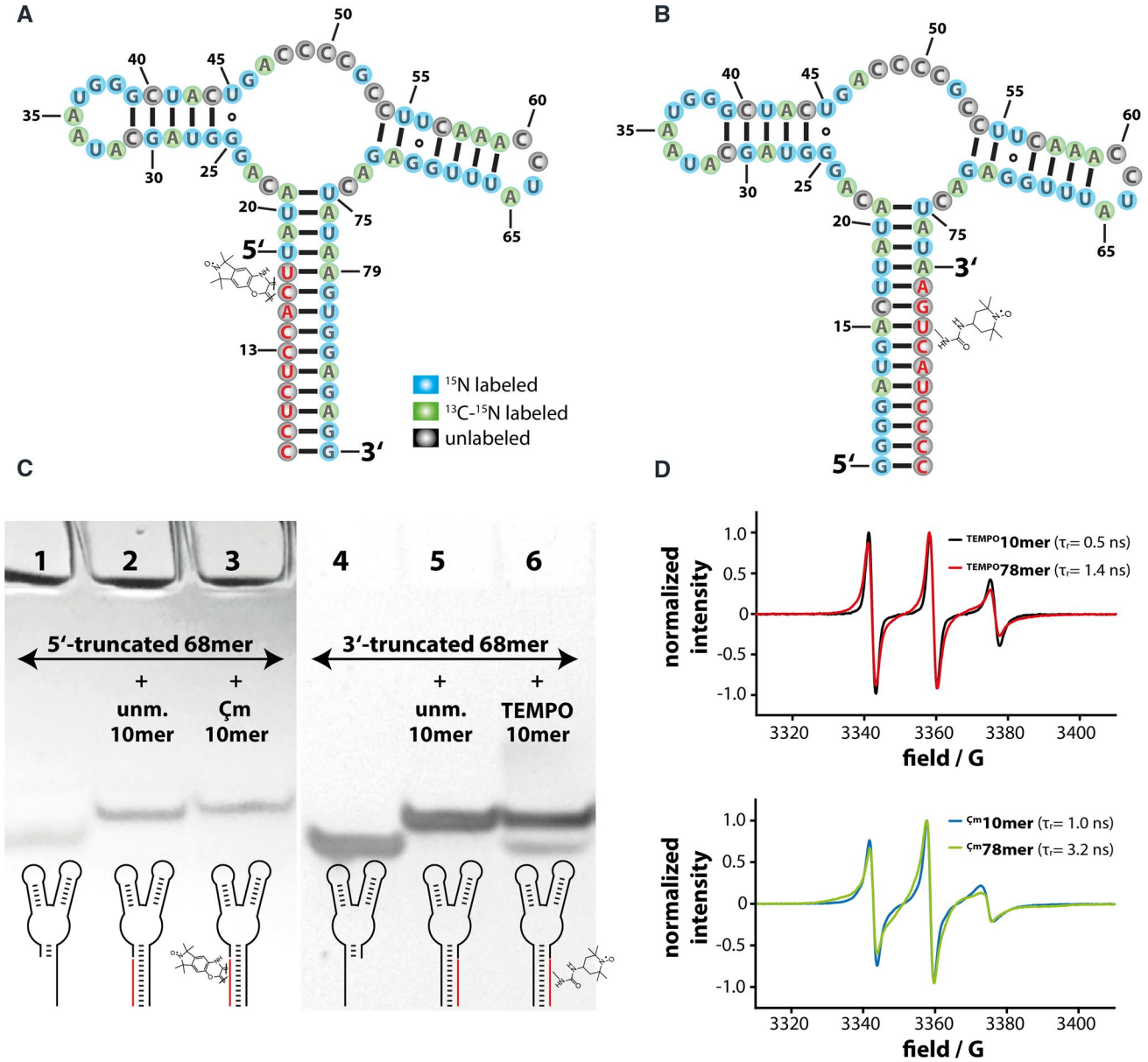

Fig. 1 **a** Secondary structure of 5′-truncated 68mer + paramagnetic ^{Çm}10mer. **b** Secondary structure of 3′-truncated 68mer + paramagnetic ^{TEMPO}10mer. **c** 12% native polyacrylamide gel illustrating complex stability. *1*: I-A 5′-truncated 68mer; *2*: I-A 5′-truncated 68mer + 10mer; *3*: I-A 5′-truncated 68mer + ^{Çm}10mer; *4*: I-A 3′-truncated 68mer; *5*: I-A 3′-truncated 68mer + 10mer; *6*: I-A 3′-truncated 68mer + ^{TEMPO}10mer. Gels were run at 277 K for 6 h at a maximal power of 1.5 W. **d** CW-EPR spectra: ^{TEMPO}10mer fragment (*black*) and in complex with 68mer forming the ^{TEMPO}78mer construct (*red*), and CW-EPR spectra of the ^{Çm}10mer fragment (*blue*) and in complex with 68mer RNA forming the ^{Çm}78mer system (*green*). Rotational correlation times were determined by EasySpin least square fitting (Stoll and Schweiger 2006) and are indicated accordingly

PRE rates were correlated to electron-nucleus distances extracted from the crystal structure (3SKI) (Fig. 3a, c) and to the residue number (Fig. 3b, d). The correlation plots display a clear trend of ^{1}H-Γ_2 reduction with increasing SL—nucleus distances. Fitting was performed using a power function $a \times x^{-b}$. Our data follows a distance dependence of $r^{-6.1\pm0.7}$ for the TEMPO labeled 78mer and $r^{-5.9\pm1.1}$ for the Çm labeled complex, which is in good agreement with the expected NMR parameter. Overlapping peaks did not yield reliable PRE intensities and were therefore excluded from analysis. U17 and U18 show significantly lower PRE rates than theoretically

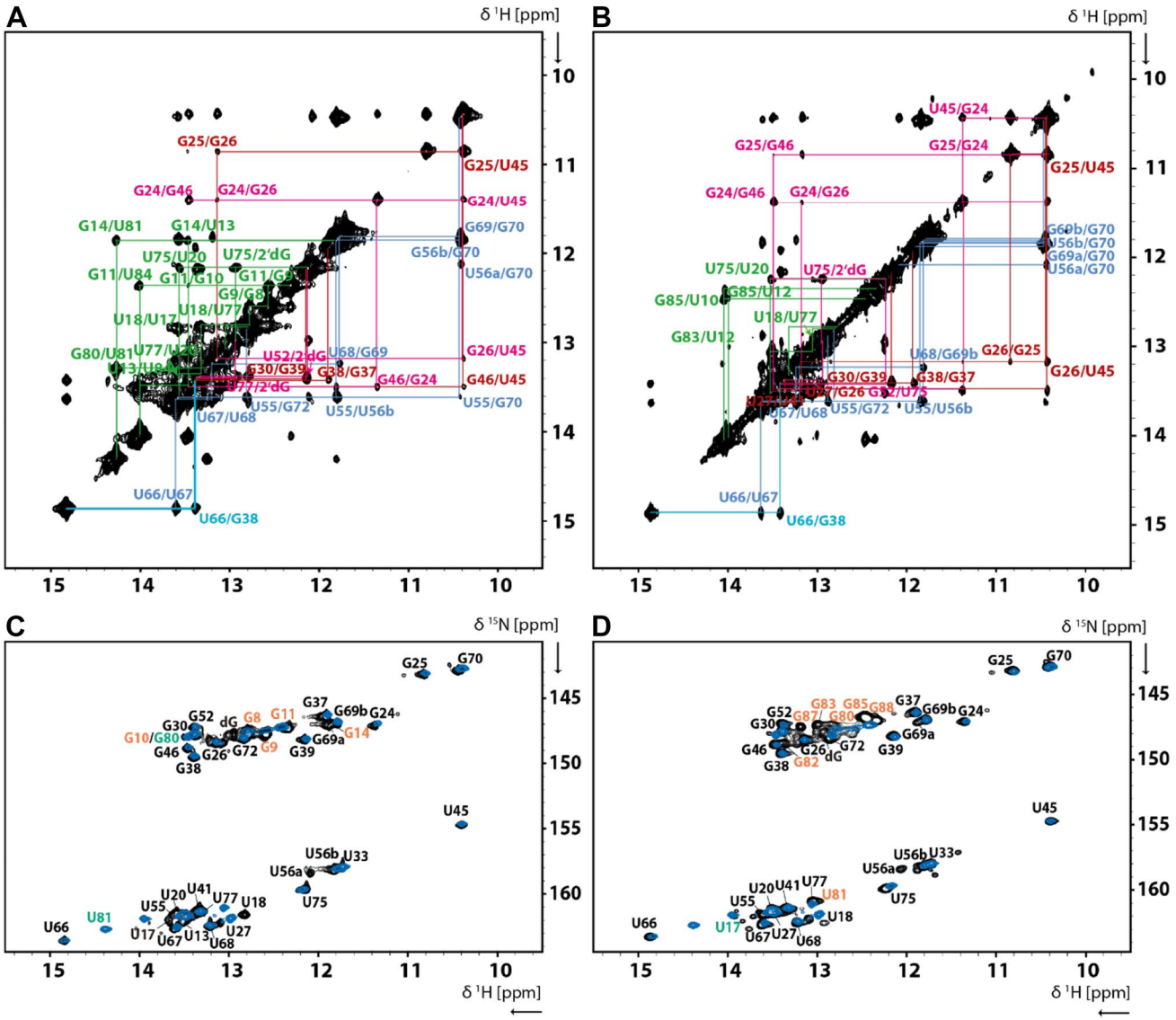

Fig. 2 NMR characterization and overlay of HSQC spectra of the wt-aptamer and the ligand-bound I-A 68 + 10mer complexes truncated at the 3′- or 5′-end, respectively. All NMR samples contained 2 equivalents of 10mer, 2 equivalents of 2′dG, and 8 equivalents of Mg^{2+} in NMR buffer. Spectra were acquired at 283 K with mixing times of 150 ms. **a** NOESY spectrum of the 3′-truncated 68 + 10mer system in the ligand-bound complex and a sample concentration of 400 µM, recorded at 700 MHz. The assignment of P1 stem is marked in *green*, P2 in *dark red*, and P3 is color coded in *blue*. The loop–loop interactions of L2 and L3 are highlighted in *turquoise*, and the interactions of the binding pocket are marked in *magenta*; **b** Overlay of ^{1}H–^{15}N-HSQC (IA-70mer, stabilized wild-type, *blue*) and ^{1}H–^{15}N-TROSY (68 + ^{TEMPO}10mer, diamagnetic state, *black*) at 800 MHz. *Orange labels* indicate nucleotides that are either not present in the wild-type or shifted due to sequential alterations in the two aptamers. Unlabeled residues containing the ^{15}N isotope only in natural abundance are color-coded in *green*. **c** NOESY spectrum of the 5′-truncated 68 + ^{Cm}10mer system in the ligand-bound complex and a sample concentration of 350 µM, recorded at 900 MHz. The color-coding for assignment is identical to (**a**). **d** Overlay of ^{1}H–^{15}N-HSQC (I-A-70mer, stabilized wild-type, *blue*) and ^{1}H–^{15}N-TROSY (68 + ^{Cm}10mer, diamagnetic state, *black*) at 800 MHz

calculated: U17 (16.05 vs. 588.12 Hz); U18 (29.78 vs. 147.99 Hz). The reason for that could be that both residues are located at the terminal region of the hybridized oligomer. A slightly weaker base pair interaction in addition to internal dynamics could cause the lower values, which has a very pronounced effect on the transversal rates in close proximity of the spin label (<13 Å), due to the r^{-6} distance dependence of the PRE rate.

Electron-nucleus distances calculated using the I-A aptamer crystal structure were correlated to the experimentally determined PRE distances (Fig. 4). The agreement of the experimental PRE data with the crystal structure is

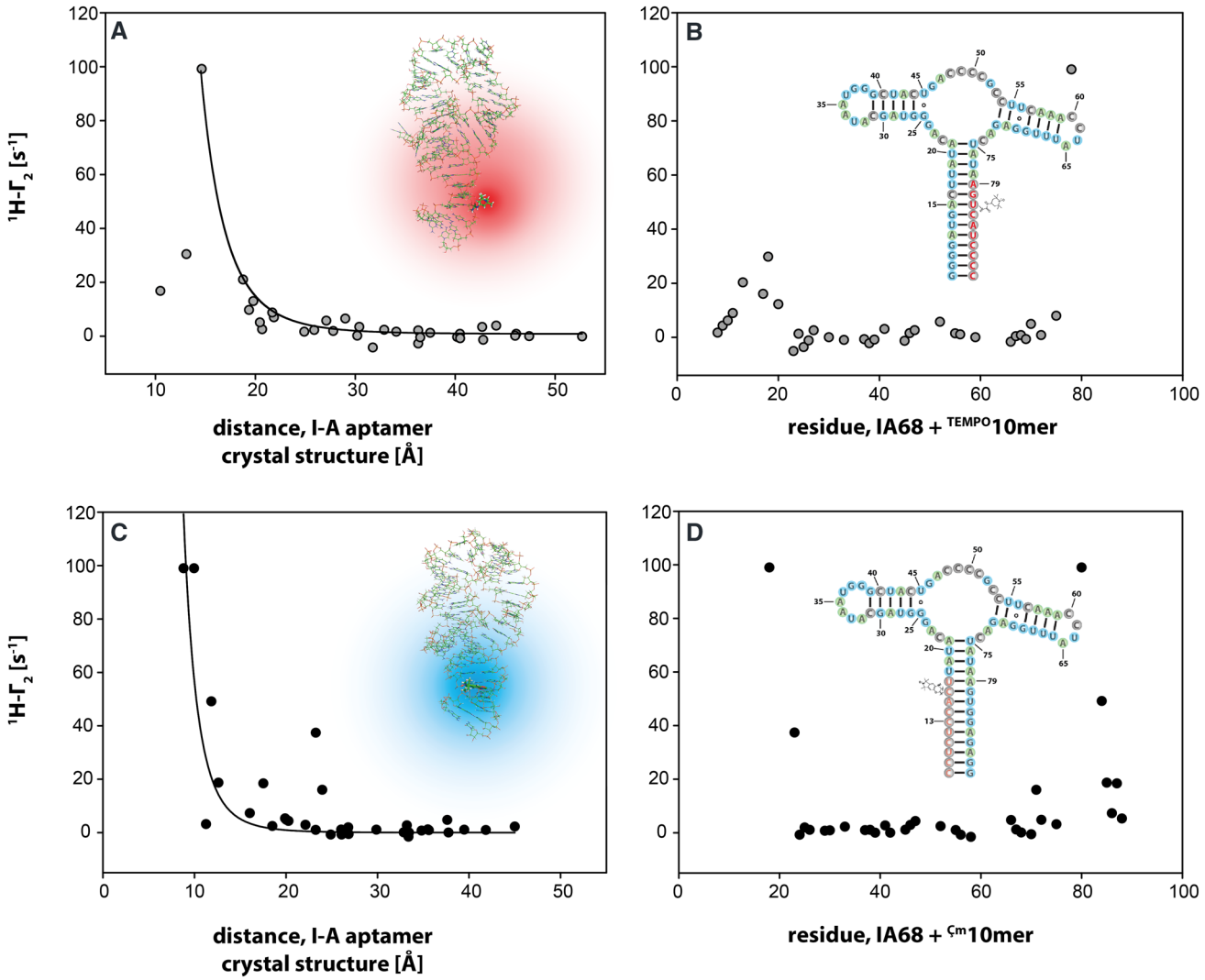

Fig. 3 Transverse PRE rates determined in construct 68 + ^{TEMPO}10mer and construct 68 + ^{Çm}10mer, respectively. **a, c** Illustrate the ^1H_N-Γ$_2$ and ^1H_C-Γ$_2$ rates calculated from imino and adenine-H2 protons for both systems correlated with distances extracted from the crystal structure of the I-A aptamer. Fitting of data points was performed with a power function $a \times x^{-b}$. Errors of the rates were calculated from S/N ratios acc. to (Iwahara et al. 2007a) and can be reviewed in Supplementary Table S6 and S7. **b, d** Illustrate the ^{1}H-Γ$_2$ rates of the I-A 68 + ^{TEMPO}10mer (**b**) and I-A 68 + ^{Çm}10mer (**d**) correlated with the residue number

slightly better for the system with rigid Çm group (94.1 vs. 88.9%).

Discussion and conclusions

In this contribution, we compared the quality of PRE data derived from two spin labels with different dynamic properties in large RNAs using the I-A riboswitch aptamer domain (78 nt) from *M. florum*. To optimize formation of a stable complex, we engineered oligomer fragments with favorably low hybridization energies and high palindromic barriers. In addition, we investigated differences in PRE data quality of the rigid spin label (Çm) and the flexible ^{Ureido}TEMPO-group (UTM).

Imino- vs. aromatic protons for PRE determination

The majority of the PRE-derived long-range restraints in our studies were calculated from imino proton intensities. However, imino protons can be subject to solvent exchange processes, which could alter the intensities and potentially generate imprecise PRE data. Typically, imino exchange rates are determined by longitudinal inversion recovery

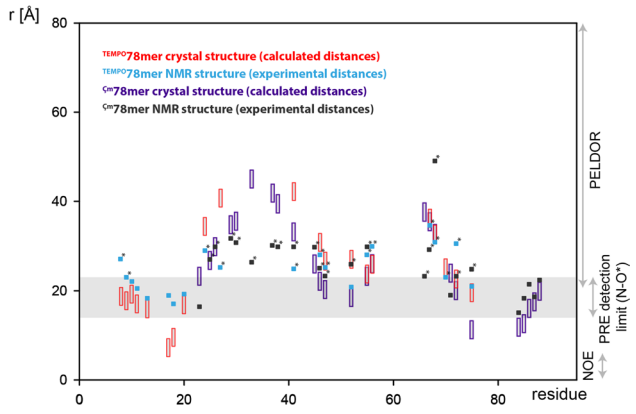

Fig. 4 Correlation of experimentally determined distances with calculated distances on the crystal structure (3SKI). *Red* SL-nucleus distance simulated from the TEMPO-labeled crystal structure. *Light blue* SL-nucleus distance experimentally determined on the TEMPO-labeled construct by NMR. *Purple* SL-nucleus distance simulated from the Çm-labeled crystal structure. *Dark grey* SL-nucleus distance experimentally determined on the Çm-labeled construct by NMR. The *grey box* indicates the PRE detection limit of nitroxide spin labels (~14–23 Å). The *asterisks* indicate experimental distances which would correspond to distances of at least 23 Å in structure calculations, hence rates below 5 Hz, therefore within the error of signal-to-noise

experiments. The corresponding apparent exchange rates of base paired imino protons cover a range between ~3 and 6 Hz (Fürtig 2007; Buck et al. 2007), carrying an additional term due to dipolar cross-relaxation. Taking this contribution into account, the net imino proton exchange rate, $k_{ex,net}$ (T) is within a range of <1 Hz (Steinert et al. 2012) and much smaller. Consequently, the PRE rates determined on imino rates for sites in stable secondary structure elements should not be significantly altered by solvent exchange. This assumption was supported by PRE data obtained from non-exchangable aromatic protons (Ade-H2). Data for aromatic protons are consistent with PRE-derived distances from imino protons (Supplementary Table S4). Hence, we conclude that $^{1}H_N$-Γ_2 rates can be reliably determined based on imino-protons. Regarding practical applications, imino protons represent easier targets for PRE applications. In contrast, the biochemical, experimental, and computational effort for PRE analysis of aromatic protons is much higher in systems of comparable sizes (≥70 nt). In particular, assignment of imino resonances is not as time-consuming as characterization of aromatic protons, and aromatic resonances are subject to a smaller range of signal dispersion, compared to imino protons.

Flexible UTM vs. rigid Çm spin label

As expected, the rigid Çm label incorporated via Watson–Crick base pairing exhibits a higher degree of structural homology to the I-A aptamer crystal structure (3SKI) (Supplementary Table S6, S7). We conclude that the rigid Çm label yields higher quality PRE data compared to the flexible Ureido-linked TEMPO group. However, flexible TEMPO labels have been widely applied in the past for structural studies and doubtlessly produce useful long-range data. The additional degree of freedom needs to be accounted for by increasing the bounds for structure calculation, while rigidly attached spin labels, as the Çm group are expected to produce more precise structural data.

Table 1 Summary of the quantity of possible restraints from different spin labeling sites, considering evaluation of imino protons and aromatic ^{13}C coupled protons

	14–23 Å ^{15}N	14–23 Å ^{13}C	<14 Å ^{15}N	<14 Å ^{13}C
U27	7	4	0	1
U41	3	2	0	0
U45	4	6	3	3
U55	1	2	0	2
U77	8	3	2	7
U20	7	4	1	6
U68	5	5	0	5
C40	3	5	0	2
C43	4	5	5	4

Area of application

This spin labeling approach works well if the area of interest is locally restricted. Distances within the affected area of the spin label can easily be evaluated and we showed that 7–9 specific restraints can be acquired per spin label. For de novo structure elucidation, however, one must introduce more spin label sites to be able to derive the global folding of the RNA. Therefore, we analyzed different possible spin labeling sites for the ^{Ureido}TEMPO group. Under the assumption that one part of the RNA is spin- but not isotope-labelled and the other part is only isotope labelled, we considered several constructs that are accessible by ligation (for the exact labeling scheme see SI). Table 1 summarizes the number of possible restraints in the range of the spin label. The number of available specific restraints per spin label varies from 11 for the ^{Ureido}TEMPO-U27 to 3 for the ^{Ureido}TEMPO-U55. The isotope labeling scheme plays a crucial role for the number of detectable restraints, since only part of the RNA is isotope labelled. For example, for the spin label in the U55 position nine distances would not be detectable due to the lack of isotope labeling of those nuclei. With multiple spin labels distributed throughout the RNA, the general folding of the RNA aptamer could be mapped. As the experimentally determined restraints cover mostly the P1 helix of the aptamer, the additional spin label

positions should cover the P2 and P3 helices. Suitable positions would be U20, U68 or C40 (for more details see Supporting Figure S8).

Conclusion

The presented data cross validate the approach of noncovalent spin labeling by implementing spin labels to different RNA systems containing helical segments of at least ten base pairs. We further showed the applicability of the rigid Çm spin label in addition to the flexible Ureido-TEMPO group. In the context of structural studies, the rigid Çm label yields more accurate PRE data due to the absence of conformational flexibility within the paramagnetic group. However, considerable experimental effort is required for Çm labeling, whereas ^{Ureido}TEMPO labeling can be performed in standard biochemical laboratories. For structural studies, multiple spin-labeled samples to cover distance space up to 23 Å are required. Assembly of these samples by noncovalent spin labeling through hybridization of nucleic acid single strands decreases the demand on biochemical ligation. Both isotope labeled strands (Helmling et al. 2016) and chemically synthesized strands containing spin labels have now become routinely available, allowing facile application of the proposed strategy.

Acknowledgements We are grateful to Dr. Christian Richter for excellent assistance with the NMR-spectrometers. This work was supported by Stiftung Polytechnische Gesellschaft and DFG-funded CRC902. H.S. and T.P. are members of the DFG-funded cluster of excellence: macromolecular complexes. BMRZ is supported by the state of Hessen.

References

Allerson CR, Chen SL, Verdine GL (1997) A chemical method for site-specific modification of RNA: the convertible nucleoside approach. J Am Chem Soc 119:7423–7433. doi:10.1021/ja962858n

Barthelmes K, Reynolds AM, Peisach E et al (2011) Engineering encodable lanthanide-binding tags into loop regions of proteins. J Am Chem Soc 133:808–819. doi:10.1021/ja104983t

Battiste JL, Wagner G (2000) Utilization of site-directed spin labeling and high-resolution heteronuclear nuclear magnetic resonance for global fold determination of large proteins with limited nuclear overhauser effect data. BioChemistry 39:5355–5365. doi:10.1021/bi000060h

Bertini I, Luchinat C (1999) New applications of paramagnetic NMR in chemical biology. Curr Opin Chem Biol 3:145–151. doi:10.1016/S1367-5931(99)80026-X

Bertini I, Luchinat C, Parigi G, Pierattelli R (2008) Perspectives in paramagnetic NMR of metalloproteins. Dalton Trans. doi:10.1039/b719526e

Bertini I, Luchinat C, Nagulapalli M et al (2012) Paramagnetic relaxation enhancement for the characterization of the conformational heterogeneity in two-domain proteins. Phys Chem Chem Phys 14:9149–9156. doi:10.1039/c2cp40139h

Bertram K, Agafonov DE, Liu W-T et al (2017) Cryo-EM structure of a human spliceosome activated for step 2 of splicing. Nature 542:318–323. doi:10.1038/nature21079

Blundell TL, Fernández-Recio J (2006) Cell biology: brief encounters bolster contacts. Nature 444:279–280. doi:10.1038/nature05306

Breaker RR (2011) Prospects for riboswitch discovery and analysis. Mol Cell 43:867–879. doi:10.1016/j.molcel.2011.08.024

Buck J, Fürtig B, Noeske J et al (2007) Time-resolved NMR methods resolving ligand-induced RNA folding at atomic resolution. Proc Natl Acad Sci USA 104:15699–15704. doi:10.1073/pnas.0703182104

Büttner L, Seikowski J, Wawrzyniak K, et al (2013) Synthesis of spin-labeled riboswitch RNAs using convertible nucleosides and DNA-catalyzed RNA ligation. Bioorg Med Chem. doi:10.1016/j.bmc.2013.04.007

Caron M, Dugas H (1976) Specific spin-labeling of transfer ribonucleic acid molecules. Nucleic Acids Res 3:19–34

Carter A, Clemons W, Brodersen D et al (2000) Functional insights from the structure of the 30S ribosomal subunit and its interactions with antibiotics. Nature 407:340–348. doi:10.1038/35030019

Clore GM, Iwahara J (2009) Theory, practice, and applications of paramagnetic relaxation enhancement for the characterization of transient low-population states of biological macromolecules and their complexes. Chem Rev 109:4108–4139. doi:10.1021/cr900033p

Donaldson LW, Skrynnikov NR, Choy W et al (2001) Structural characterization of proteins with an attached ATCUN motif by paramagnetic relaxation enhancement NMR spectroscopy. Society 123:9843–9847. doi:10.1021/ja011241

Dvoretsky A, Gaponenko V, Rosevear PR (2002) Derivation of structural restraints using a thiol-reactive chelator. FEBS Lett 528:189–192. doi:10.1016/S0014-5793(02)03297-0

Edwards TE, Sigurdsson ST (2007) Site-specific incorporation of nitroxide spin-labels into 2′-positions of nucleic acids. Nat Protoc 2:1954–1962. doi:10.1038/nprot.2007.273

Edwards TE, Okonogi TM, Robinson BH, Sigurdsson ST (2001) Site-specific incorporation of nitroxide spin-labels into internal sites of the TAR RNA; structure-dependent dynamics of RNA by EPR spectroscopy. Supplementary. J Am Chem Soc 123:1527–1528

Fürtig B (2007) NMR-study of dynamic structural transitions in RNA-molecules. Dissertation, Goethe University, Frankfurt am Main

Gaponenko V, Howarth JW, Columbus L et al (2000) Protein global fold determination using site-directed spin and isotope labeling. Protein Sci 9:302–309. doi:10.1110/ps.9.2.302

Garca de la Torre J, Huertas ML, Carrasco B (2000) HYDRONMR: prediction of NMR relaxation of globular proteins from atomic-level structures and hydrodynamic calculations. J Magn Reson 147:138–146. doi:10.1006/jmre.2000.2170

Gillespie JR, Shortle D (1997) Characterization of long-range structure in the denatured state of staphylococcal nuclease. I. Paramagnetic relaxation enhancement by nitroxide spin labels. J Mol Biol 268:158–169. doi:10.1006/jmbi.1997.0954

Goddard TD, Kneller DG (2008) SPARKY 3. University of California, San Francisco

Graham B, Loh CT, Swarbrick JD et al (2011) DOTA-amide lanthanide tag for reliable generation of pseudocontact shifts in protein NMR spectra. Bioconjug Chem 22:2118–2125. doi:10.1021/bc200353c

Guan J-Y, Keizers PHJ, Liu W-M et al (2013) Small-molecule binding sites on proteins established by paramagnetic NMR spectroscopy. J Am Chem Soc 135:5859–5868. doi:10.1021/ja401323m

Helmling C, Bessi I, Wacker A et al (2014) Noncovalent spin labeling of riboswitch RNAs to obtain long-range structural NMR restraints. ACS Chem Biol 9:1330–1339. doi:10.1021/cb500050t

Höbartner C, Sicoli G, Wachowius F et al (2012) Synthesis and characterization of RNA containing a rigid and nonperturbing cytidine-derived spin label. J Org Chem 77:7749–7754. doi:10.1021/jo301227w

Hubbell WL, López CJ, Altenbach C, Yang Z (2013) Technological advances in site-directed spin labeling of proteins. Curr Opin Struct Biol 23:725–733. doi:10.1016/j.sbi.2013.06.008

Iwahara J, Schwieters CD, Clore GM (2004) Characterization of nonspecific protein-DNA interactions by 1 H paramagnetic relaxation enhancement. J Am Chem Soc 126:12800–12808. doi:10.1021/ja046246b

Iwahara J, Tang C, Clore GM (2007a) Practical aspects of 1 H transverse paramagnetic relaxation enhancement measurements on macromolecules. J Magn Reson 184:185–195

Iwahara J, Tang C, Clore GM (2007b) Practical aspects of 1 H transverse paramagnetic relaxation enhancement measurements on macromolecules. J Magn Reson 184:185–195. doi:10.1016/j.jmr.2006.10.003

Kamble NR, Gränz M, Prisner TF et al (2016) Noncovalent and site-directed spin labeling of duplex RNA. Chem Commun 52:14442–14445. doi:10.1039/C6CC08387K

Kim JN, Roth A, Breaker RR (2007) Guanine riboswitch variants from *Mesoplasma florum* selectively recognize 2′-deoxyguanosine. Proc Natl Acad Sci USA 104:16092–16097. doi:10.1073/pnas.0705884104

Kosen PA (1989) Spin labeling of proteins. Methods Enzymol 177:86–121. doi:10.1016/0076-6879(89)77007-5

Krstic I, Endeward B, Margraf D et al (2012) Structure and dynamics of nucleic acids. Top Curr Chem 321:159–198

Lebars I, Vileno B, Bourbigot S, et al (2014) A fully enzymatic method for site-directed spin labeling of long RNA. Nucleic Acids Res. doi:10.1093/nar/gku553

Li P, Kirkpatrick J, Carlomagno T (2009) An efficient strategy for the determination of the three-dimensional architecture of ribonucleoprotein complexes by the combination of a few easily accessible NMR and biochemical data: intermolecular recognition in a U4 spliceosomal complex. J Mol Biol 388:283–298. doi:10.1016/j.jmb.2009.03.001

Liang BY, Bushweller JH, Tamm LK (2006) Site-directed parallel spin-labeling and paramagnetic relaxation enhacement in structure determination of membrane proteins by solution NMR spectroscopy. J Am Chem Soc 128:4389–4397

Lorenz R, Bernhart SH, Zu Siederdissen CH et al (2011) ViennaRNA Package 2.0. Algorithms Mol Biol 6:26. doi:10.1186/1748-7188-6-26

Macosko JC, Pio MS, Tinoco I, Shin YK (1999) A novel 5 displacement spin-labeling technique for electron paramagnetic resonance spectroscopy of RNA. RNA 5:1158–1166. doi:10.1017/S1355838299990830

Madl T, Güttler T, Görlich D, Sattler M (2011) Structural analysis of large protein complexes using solvent paramagnetic relaxation enhancements. Angew Chem Int Ed 50:3993–3997. doi:10.1002/anie.201007168

Mourão A, Bonnal S, Soni K et al (2016) Structural basis for the recognition of spliceosomal SmN/B/B' proteins by the RBM5 OCRE domain in splicing regulation. eLife. doi:10.7554/eLife.14707

Mückstein U, Tafer H, Hackermüller J et al (2006) Thermodynamics of RNA–RNA binding. Bioinformatics 22:1177–1182. doi:10.1093/bioinformatics/btl024

Nagahara S, Murakami A, Makino K (1992) spin-labeled oligonucleotides site specifically labeled at the internucleotide linkage. separation of stereoisomeric probes and EPR spectroscopical detection of hybrid formation in solution. Nucleosides Nucleotides 11:889–901. doi:10.1080/07328319208021747

Otting G (2010a) Protein NMR using paramagnetic ions. Annu Rev Biophys 39:387–405. doi:10.1146/annurev.biophys.093008.131321

Otting G (2010b) Protein NMR using paramagnetic ions. Annu Rev Biophys 39:387–405. doi:10.1146/annurev.biophys.093008.131321

Pintacuda G, Moshref A, Leonchiks A et al (2004) Site-specific labelling with a metal chelator for protein-structure refinement. J Biomol NMR 29:351–361. doi:10.1023/B:JNMR.0000032610.17058.fe

Piton N, Mu Y, Stock G et al (2007) Base-specific spin-labeling of RNA for structure determination. Nucleic Acids Res 35:3128–3143. doi:10.1093/nar/gkm169

Qin PZ, Hideg K, Feigon J, Hubbell WL (2003) Monitoring RNA base structure and dynamics using site-directed spin labeling. BioChemistry 42:6772–6783. doi:10.1021/bi027222p

Ramos A, Varani G (1998) A new method to detect long-range protein–RNA contacts: NMR detection of electron–proton relaxation induced by nitroxide spin-labeled RNA. J Am Chem Soc 120:10992–10993. doi:10.1021/ja982496e

Saha S, Jagtap AP, Sigurdsson ST (2015) Site-directed spin labeling of 2′-amino groups in RNA with isoindoline nitroxides that are resistant to reduction. Chem Commun 51:13142–13145. doi:10.1039/c5cc05014f

Sashital DG, Butcher SE (2007) Ribozymes and RNA catalysis. Royal Society of Chemistry, Cambridge

Schmidt PG, Kuntz ID (1984) Distance measurements in spin-labeled lysozyme. BioChemistry 23:4261–4266. doi:10.1021/bi00313a038

Serganov A, Nudler E (2013) A decade of riboswitches. Cell 152:17–24

Shelke SA, Sigurdsson ST (2010) Noncovalent and site-directed spin labeling of nucleic acids. Angew Chemie Int Ed 49:7984–7986. doi:10.1002/anie.201002637

Shelke SA, Sigurdsson ST (2012) Site-directed spin labelling of nucleic acids. Eur J Org Chem 2012:2291–2301. doi:10.1002/ejoc.201101434

Shelke SA, Sandholt GB, Sigurdsson ST (2014) Nitroxide-labeled pyrimidines for non-covalent spin-labeling of abasic sites in DNA and RNA duplexes. Org Biomol Chem 12:7366. doi:10.1039/C4OB01095G

Sicoli G, Wachowius F, Bennati M, Höbartner C (2010) Probing secondary structures of spin-labeled RNA by pulsed EPR spectroscopy. Angew Chem Int Ed 49:6443–6447. doi:10.1002/anie.201000713

Spaltenstein A, Robinson BH, Hopkins PB (1988) A rigid and nonperturbing probe for duplex DNA motion. J Am Chem Soc 110:1299–1301. doi:10.1021/ja00212a053

Steinert HS, Rinnenthal J, Schwalbe H (2012) Individual base-pair stability of DNA and RNA studied by NMR-detected solvent exchange. Biophys J 102:2564–2574. doi:10.1016/j.bpj.2012.03.074

Stoldt M, Wöhnert J, Görlach M, Brown LR (1998) The NMR structure of Escherichia coli ribosomal protein L25 shows homology to general stress proteins and glutaminyl-tRNA synthetases. EMBO J 17:6377–6384. doi:10.1093/emboj/17.21.6377

Stoll S, Schweiger A (2006) EasySpin, a comprehensive software package for spectral simulation and analysis in EPR. J Magn Reson 178:42–55. doi:10.1016/j.jmr.2005.08.013

Tang C, Iwahara J, Clore GM (2006) Visualization of transient encounter complexes in protein–protein association. Nature 444:383–386. doi:10.1038/nature05201

Tang C, Schwieters CD, Clore GM (2007) Open-to-closed transition in apo maltose-binding protein observed by paramagnetic NMR. Nature 449:1078–1082. doi:10.1038/nature06232

Tang C, Ghirlando R, Clore GM (2008) Visualization of transient ultra-weak protein self-association in solution using paramagnetic relaxation enhancement. J Am Chem Soc 130:4048–4056. doi:10.1021/ja710493m

Ubbink M, Worrall J a R, Canters GW et al (2002) Paramagnetic resonance of biological metal centers. Annu Rev Biophys Biomol Struct 31:393–422. doi:10.1146/annurev.biophys.31.091701.171000

Volkov AN, Worrall J a R, Holtzmann E, Ubbink M (2006) Solution structure and dynamics of the complex between cytochrome c and cytochrome c peroxidase determined by paramagnetic NMR. Proc Natl Acad Sci 103:18945–18950. doi:10.1073/pnas.0603551103

Wöhnert J, Franz KJ, Nitz M et al (2003) Protein alignment by a coexpressed lanthanide-binding tag for the measurement of residual dipolar couplings. J Am Chem Soc 125:13338–13339. doi:10.1021/ja036022d

Wunderlich CH, Huber RG, Spitzer R et al (2013) A novel paramagnetic relaxation enhancement tag for nucleic acids: a tool to study structure and dynamics of RNA. ACS Chem Biol. doi:10.1021/cb400589q